Biophysical Journal, Volume 96

Supporting Material

K^+/Na^+ Selectivity in Toy Cation Binding Site Models is Determined by the 'Host'

David L. Bostick, Karunesh Arora, and Charles L. Brooks III

Supplementary Material

K^+/Na^+ Selectivity in Toy Cation Binding Site Models is Determined by the 'Host'

David L. Bostick, Karunesh Arora, and Charles L. Brooks III*
The University of Michigan
Department of Chemistry and Program in Biophysics
930 N. University Ave.
Ann Arbor, Michigan 48109

* To whom all correspondence should be addressed: brookscl@umich.edu

Supplementary Methods

Simulations of K^+/Na^+ in Toy Model Environments

Toy models were simulated at constant temperature (298 K) using Langevin dynamics. All calculations were performed with a time step of 1 fs. Full interactions were included for all molecular species in each model. Configurations were saved every 0.1 ps for later analysis. All simplified toy models were comprised of a single cation surrounded by $N_{toy} \leq 8$ dipolar ligands under the influence of an applied external field $U^{toy}_{K/Na}$, where the ligands were taken to be either water molecules or fictitious linear dipolar moieties. Fictitious linear carbonyl-like moieties were described by either standard (1) or modified (2,3) CHARMM ion and carbonyl parameters (Table S2). Water molecules were described by the variant TIP3P water model (4) implemented in CHARMM (1) in combination with modified ion parameters (2,3,5,6) (Table S2). The ligand dipole moment was varied in toys employing the carbonyl-like model by reassigning the partial charge on the carbon and oxygen nuclear sites. In order to investigate the effect of a "linear" shape, versus the "bent" shape of a water molecule, on selectivity in the toy (as in Fig. 3B), we also investigated a "crippled" water molecule, where the TIP3P dipole (2.3 D) and dispersive oxygen and hydrogen interactions were maintained, but where one of the hydrogen sites was removed. The charge was redistributed (each site with a partial charge of $\delta = \pm 0.4978e$ separated by a distance of 0.9752 Å) across this fictitious linear H–O molecule in order to maintain the dipole moment of TIP3P.

Three different classes of spherically symmetric potential, $U^{toy}_{K/Na}$, were employed to probe the effects of different types of structural constraints on K^+/Na^+ selectivity. Irrespective of the specific functional form of each class of $U^{toy}_{K/Na}$ investigated, all of the toy models of this work meet the following two criteria, as outlined previously (5-7): (*criterion 1*) U^{toy} confines the N_{toy} included ligands in the vicinity of K^+/Na^+, and (*criterion 2*) does not prevent the radial "collapse" of the included N_{toy} ligands to accommodate the central cation's size. The first two classes of toy were simulated using

the TINKER package (8). We carried out alchemical transformation of the Hamiltonian describing each of our various models by performing a sequence of eleven 500 ps simulations at coupling parameter values, $\lambda = \{0.0,0.1,0.2,\cdots,1.0\}$. This allowed a 20-step perturbation for each toy in which the result for each step was calculated using the latter 200 ps of each simulated window.

The first class of toy model investigated was explained in previous works (5-7,9), and incorporates a volume confining restraint that prevents the included ligands from traveling significantly more than 3.5 Å away from the central cation. Since this toy aims to capture the "essential" features of the canonical 8-fold binding site via a uniformly prescribed volume confinement, we warmly refer to it as the "naive" toy model. For this class, we utilized two types of confining potential. One type [utilized in references (5-7)] was a half-harmonic restraint [employed by the "restrain-distance" directive in TINKER] acting on the oxygen atoms of the included ligands. Harmonic constants tested varied between 10^2-10^3 kcal/mol/Å^2. Smaller harmonic constants gave rise to similar selective free energies, but were less able to confine all included ligands to within the specified radius (3.5 Å). The other type of confining potential [utilized in reference (9)] was a Lennard-Jones (LJ) restraint [employed by the "wall" directive in TINKER] acting on all nuclear sites of the included ligands.

We found that, in the case of water molecules (and carbonyl-like groups with a large assigned dipole moment – see Fig. S1), the naive toy model (employing a 3.5 Å restraint) with Na^+ as the central ion and $N_{toy} = 8$ ligands allowed the confined droplet to "buckle" or relax and form a distinct second solvation shell (Figs. 3C and S2-S3) – a property that is not observed in the pair correlation functions derived from CHARMM simulations of KcsA (5,6,10,11). The original intention of the naive toy model was to probe the selective effect of solely confining all N_{toy} included ligands to the first coordination shell of the central cation without necessarily targeting the exact structure of site S2. Thus, we invented a second class of toy in which $U_K^{toy} \neq U_{Na}^{toy}$. In determining $\Delta F_{K \to Na}$ using FEP, the alchemical transformation $U_K^{toy} \to U_{Na}^{toy}$ followed the alchemical transformation $K^+ \to Na^+$ as separate calculations. The potentials $U_{K/Na}^{toy}$ possessed the same functional form as the naive toys, but the restraint was radially adjusted (depending on the identity of the central cation – K^+ or Na^+) so as to suppress buckling to form a second solvation shell; thereby enhancing N_{toy}-fold coordination. For some, it may seem counterintuitive that a model for which $U_K^{toy} \neq U_{Na}^{toy}$ can be a justifiable representation of a host. To rationalize this second class of toy, one need only consider that the toy, either as an approximation or a hypothesis, replaces the external mean field, or external potential of mean force [hypothetically representing a solvated K^+ channel (9,12)], $W_{K/Na}^{ext}$, with the model potential function, $U_{K/Na}^{toy}$. Given this, it is expected that the host or system remainder from which the external field originates will respond to the presence of different ion-bound complexes.

The half-harmonic restraining potential utilized for this type of model was chosen to be very gentle (with a harmonic constant of 5 kcal/mol/Å^2) in comparison to that used for the naive model. As a guideline for choosing the different radial restraint for U_K^{toy} and

U_{Na}^{toy}, we used the position of the first minimum in the ion-oxygen pair correlation function observed in liquid TIP3P water (see Supplementary Text and Fig. S5). This guideline suggested radial (LJ or harmonic) boundaries of 3.5-3.6 Å and 3.0-3.2 Å for K^+ and Na^+, respectively, in the case of water-based toys. Utilizing the same guideline for carbonyl groups, analysis of a hypothetical carbonyl fluid (Supplementary Text and Fig. S5) suggested natural coordination boundaries of 4.0-4.1 Å and 3.5-3.7 Å for K^+ and Na^+, respectively. This explains why naive (3.5 Å restraint) 8-ligand carbonyl-based toys guarantee 8-fold coordination of both K^+ and Na^+ (see Figs. 3C and S4) while naive 8-ligand water-based toys do not (see Supplementary Text).

Secondary solvation shells were most effectively suppressed in water-based toys using radial restraints of 3.0 Å and 3.5 Å for the cases of Na^+ and K^+, respectively. This suppression was better achieved by the LJ restraint than by the half-harmonic restraint (Fig. S6). Using pair correlation analyses as a guideline (Fig. S5), several other water-based toys in this class were probed. All such toy models were found to yield qualitatively similar K^+/Na^+ selectivity despite their different modulation of ligand configuration (see examples in Fig. S7). For carbonyl-based toys, a single coordination shell was easily enforced using radial restraints of 3.5 Å and 4.0 Å for Na^+ and K^+, respectively (Figs. S4A-B).

Finally, we sought to probe a toy model that not only captured the qualitative feature of 8-fold coordination, but also enforced a structure comparable with site S2 of KcsA as depicted by cation-carbonyl oxygen pair correlation function analyses (5,6,10,11). Since it is already known that carbonyl ligands in the context of site S2 [as represented by CHARMM simulations of KcsA] are selective for K^+ over Na^+ (5,6,10,11), we designed a third class of toy where $U_{K/Na}^{toy}$ was adjusted to closely mimic the shape of the ion-oxygen pair density of site S2 with TIP3P water molecules (Fig. 5). We found this could be done using a full harmonic restraint between the central cation and all water oxygen sites, $U_{K/Na}^{toy} = k_{K/Na}(r - r_{K/Na})^2/2$, where $k_{K/Na}$ and $r_{K/Na}$ represent the harmonic spring constant and equilibrium distance of the potential, respectively. The pair density shape was reasonably mimicked using $k_K = 10.8$ kcal/mol/Å^2 and $r_K = 2.72$ Å for K^+, and $k_{Na} = 13.2$ kcal/mol/Å^2 and $r_{Na} = 2.80$ Å for Na^+.

For this more sophisticated model, the alchemical transformations $U_K^{toy} \rightarrow U_{Na}^{toy}$ and $K^+ \rightarrow Na^+$ were calculated simultaneously via thermodynamic integration as implemented in the GROMACS simulation package (13,14). In these calculations, the coupling parameter, λ, was linearly varied from 0 to 1 in increments of 0.05 over 21 simulations of 1 ns duration. We split the final 400 ps portion of each simulation into 10 blocks of 40 ps duration to calculate 10 sets of values for $\langle \partial H(\lambda)/\partial\lambda \rangle_\lambda$. We then integrated the resulting 10 functions over λ to obtain 10 samples of $\Delta F_{K \rightarrow Na}^{toy}$. This allowed an estimation of $\Delta F_{K \rightarrow Na}^{toy}$ with a standard error of ±0.1 kcal/mol.

Simulations of K^+/Na^+ in Bulk Water and Hypothetical Carbonyl Fluid Environments

Simulations of K^+ and Na^+ in bulk CHARMM TIP3P water and modified CHARMM hypothetical carbonyl (see Table S1) liquid environments were carried out using the same procedure as our previous work (9). The aqueous systems consisted of a single cation solvated in 2179 water molecules, and the hypothetical carbonyl liquid systems consisted of a single cation solvated in 396 carbonyl moieties. Calculations were performed with the GROMACS package using a timestep of 2 fs and configurations were saved every 0.5 ps for later analysis. Periodic boundary conditions were applied in all three dimensions. Long-range electrostatics were handled using the PME algorithm (15) with a real space cutoff of 10 Å. Other nonbonded interactions were truncated at 12 Å (10 Å for the carbonyl liquid systems). Temperature was maintained at 298 K using the Nose-Hoover scheme with an oscillatory relaxation period of 2.0 ps. The pressure was maintained at 1 atm (0 atm for the carbonyl liquid systems) using the Parrinello-Rahman coupling scheme (16,17) with a barostat time constant of 2.0 ps. The simulation box was allowed to scale isotropically in order to maintain pressure. All systems were equilibrated for 1 ns before performing production runs. The free energy change for the alchemical transformation, $K^+ \rightarrow Na^+$, was calculated for the aqueous system, which served as the reference ($\Delta F^{aq}_{K\rightarrow Na} = -18.54 \pm 0.02$ kcal/mol) for all selective free energy calculations [$\Delta\Delta F_{K\rightarrow Na} = \Delta F^{toy}_{K\rightarrow Na} - \Delta F^{aq}_{K\rightarrow Na}$, where $\Delta F^{aq}_{K\rightarrow Na}$ is the free energy difference in bulk aqueous solution and $\Delta F^{toy}_{K\rightarrow Na}$ is the free energy difference in a given toy model] employing the CHARMM force field in this work. We performed 4 ns production runs of the hypothetical carbonyl liquid systems. Trajectories derived from the aqueous and carbonyl liquid systems were used for the pair correlation function analysis shown in Fig. S5.

The free energy, $\Delta F^{aq}_{K\rightarrow Na}$, in bulk CHARMM TIP3P water was calculated using the method of thermodynamic integration. K^+ was alchemically transformed to Na^+ by linearly varying van der Waals interactions with the coupling parameter, λ, in increments of 0.05 from 0 to 1 over 21 simulations of 500 ps duration. The first 100 ps of each simulation were thrown away, and we split the final 400 ps portion of each trajectory into 10 blocks of 40 ps duration to calculate 10 sets of values for $\langle \partial H(\lambda)/\partial\lambda \rangle_\lambda$. We then integrated the resulting 10 functions over λ to obtain 10 samples of $\Delta F^{aq}_{K\rightarrow Na}$. The average and standard error over this set of values yielded $\Delta F^{aq}_{K\rightarrow Na} = -18.54 \pm 0.02$ kcal/mol.

Supplementary Text

"Packing" Considerations in Water-Based Toy Models

Analysis of ion-oxygen radial distribution functions (Fig. S5) in bulk fluid environments (for water molecules and modified CHARMM fictitious carbonyl moieties – Table S2) allowed us to understand more clearly the structural differences provided by the naive carbonyl- and water-based toy models (Figs. 3B and S2-S4). It also aided us in the design of volume-confining restraints for water-based toys in which N_{toy} more closely resembles the coordination number of K^+/Na^+ (see Methods). In fluid environments, ion-oxygen pair correlation functions suggest the differences in size, shape, and charge distribution give rise to larger cation-oxygen coordination shells (Fig. S5) for fictitious carbonyls (~4.0-4.1 Å and ~3.5-3.7 Å for K^+ and Na^+, respectively) in comparison to water molecules (~3.5-3.6 Å and ~3.0-3.2 Å for K^+ and Na^+, respectively). These packing tendencies imply that the naive 8-ligand toy (with a 3.5 Å volume-confining restraint) would naturally enforce a single coordination shell (and therefore, 8-fold coordination) for K^+ whether the ligand is taken to be a CHARMM TIP3P water molecule or a modified CHARMM carbonyl moiety. Given the broad minimum observed at ~3.5-3.7 Å for Na^+ in the hypothetical carbonyl fluid environment, one can also expect the naive 8-carbonyl toy (3.5 Å restraint) to enforce a single coordination shell for Na^+. However, since the radial coordination shell boundary for Na^+ in liquid water (~3.0-3.2 Å) is smaller than the radial restraint provided by the naive toy (3.5 Å), we can expect relaxation (or buckling) of the droplet confined by the toy, resulting in ~5-6 coordinating water molecules (Fig. S5B). Population analyses of coordination number (Fig. 3B) and radial ion-oxygen probability density analyses (Figs. S2, S3, and S4) in the naive toys fall in line with these expectations based on the solvent structure of bulk solvated K^+/Na^+ (Fig. S5).

Supplementary Tables

Table S1. Selectivity sequences in various exemplary "maxi-" type K^+ channels and KcsA as determined by various electrophysiological techniques under various conditions. We note that, irrespective of the different conditions/techniques and any possible interpretation of their respective meanings, all of the measurements have historically been considered as indicative of "good to exquisite (18)" selectivity for K^+ over Na^+. The values of $\Delta\Delta F_{K\to Na}$ (kcal/mol) in the third column can be obtained from the selectivity values, $S_{K\to Na}$, for K^+ over Na^+ in the second column using the Boltzmann relation, $\Delta\Delta F_{K\to Na} = -RT\ln(S_{K\to Na})$, where R is the gas constant and T is the temperature (RT has a value of approximately 0.59 kcal/mol at T = 298 K). Obviously, this formula relating $S_{K\to Na}$ to $\Delta\Delta F_{K\to Na}$ carries a gross/simplified interpretation irrespective of the particular experimental measurement consulted (conductance, reversal potential, or Ba^{++} dissociation from the fiter), as none of these measurements directly isolate and measure the affinity of a single ion at a single site in the filter in the same way as probed by MD simulation methodology. Recent experimental efforts have more directly measured the thermodynamics of K^+ binding in KcsA, but were unable detect Na^+ binding due to a nonconductive state adopted by the filter in the presence of Na^+ (19). The goal of this and previous works (mentioned throughout the text) have been to understand the coordinative environments that give rise to K^+-selective relative affinity. This brief table supplies an abbreviated list of quantitations of K^+-selectivity, and their associated interpretations (however simplified) in terms of affinity, that are considered "good to exquisite."

Channel Type	Selectivity Sequence	$\Delta\Delta F$
Sarcoplasmic Reticulum K+ Channel[a]		
• Rabbit	K^+ (1) > Rb^+ > Na^+ > Li^+ (0.03),Cs^+	< 2.1
• Frog	K^+ (1) > Rb^+ > Na^+ > Li^+ (0.07) >> Cs^+	< 1.6
Ca^{2+} Activated K+ Channel		
• Bovine Chromaffin Cells[b]	K^+ (1) > Rb^+ > Na^+ (~0.03),Cs^+	~2.1
• Rat Skeletal Muscle[c]	Tl^+ > Rb^+ (4.8) > K^+ (1) > Cs^+ > Na^+ (0.0007) > Li^+ (~0.0004)	~4.3
KcsA[d]	Tl^+ (3.1) > K^+ (1) > Rb^+ (0.8) > NH_4^+ (0.2) > Na^+ (~0.006)	~3.0

[a]Reference (18) – determined from measurements of channel conductance; [b]Reference (20) – determined from measurement of reversal potential; [c]Reference (21) – determined by measuring the ability of various ions to lower the dissociation rate of Ba^{++}; [d]Reference (22) – determined from measurement of reversal potential.

Table S2. Parameters for modified CHARMM ions and carbonyl groups as used in previous works (2,3,5-7). These parameters represent a modification of the standard CHARMM22 force field (1). Parameters not listed here are taken to be those of standard CHARMM22. Dispersive LJ interactions are all generated with standard arithmetic CHARMM combination rules, unless otherwise stated[a].

Atom Type	Description	Partial Charge (*e*)	LJ epsilon (kcal/mol)	LJ $R_{min}/2$ (Å)
SOD	Na^+ ion	+1	0.0469	1.40375
POT	K^+ ion	+1	0.0870	1.76375
O	Carbonyl Oxygen	-0.51	0.12	1.7
C	Carbonyl Carbon	+0.51	0.11	2.0
Special Interactions[a]				
SOD…O	—	—	0.0750200	1.64875
POT…O	—	—	0.1021763	1.821375

[a]Special Interactions are substituted for standard Na^+ and K^+ LJ interactions with carbonyl oxygen atoms.

Supplementary Figures

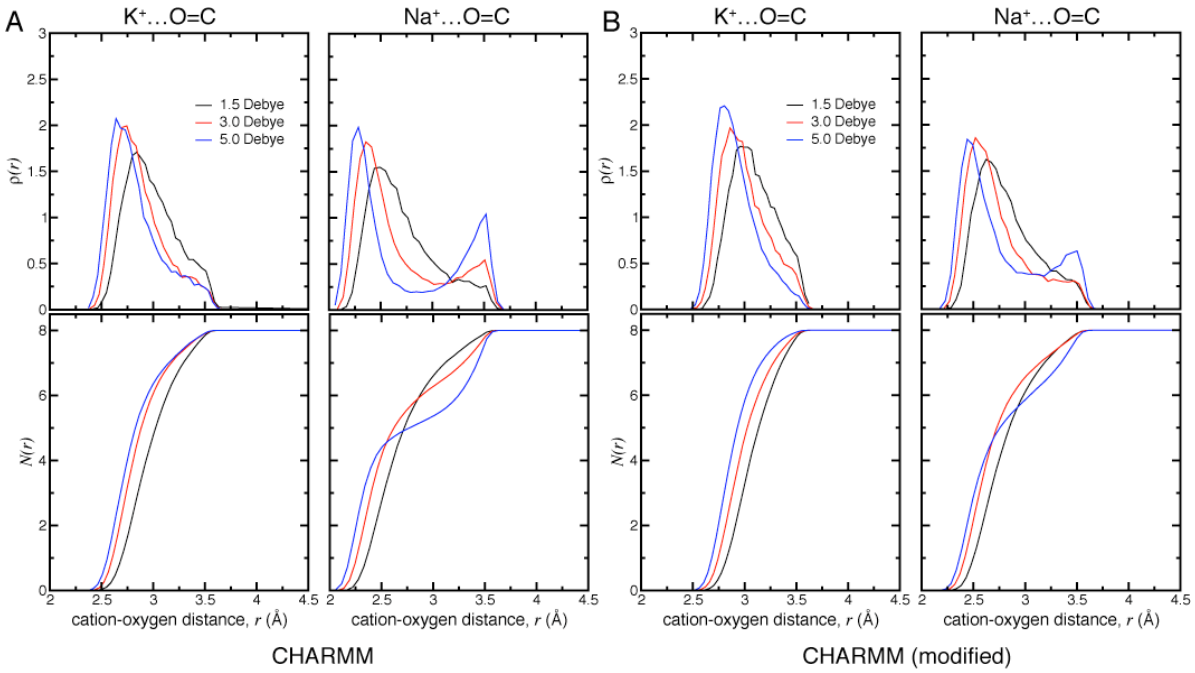

Fig S1: Structure in naive toy models comprised of carbonyl-like ligands of varying dipole. (A) ion-oxygen radial probability density (top) and cumulative number distribution (bottom) around either K^+ (left) or Na^+ (right) for carbonyl-like moieties with standard CHARMM LJ interactions. (B) ion-oxygen radial probability density (top) and cumulative number distribution (bottom) around either K^+ (left) or Na^+ (right) for carbonyl-like moieties with modified CHARMM LJ interactions (Table S1). Note that, for Na^+, in the cases of both standard and modified CHARMM parameters, decreasing the dipole moment below ~3 D does not necessarily lead to formation of a second solvation shell.

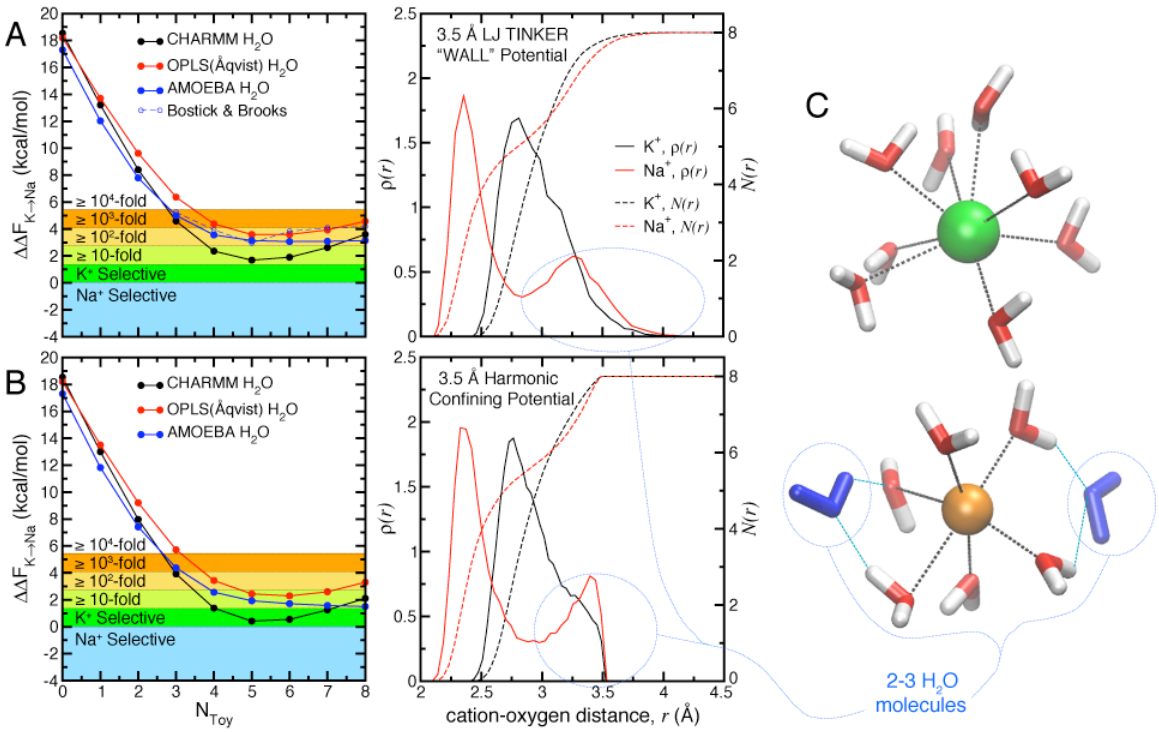

Fig S2: Results from water-based toy models implementing a "naive" 3.5 Å restraint. In order to gauge the results yielded by different water models in the naive toy model, we performed our calculations using various force fields. Our calculations included the widely used OPLS pairwise additive TIP3P water model (4) in combination with the ion parameters of Åqvist (23), the variant pairwise additive TIP3P water model implemented in CHARMM, and the more recently developed AMOEBA (24,25) ion and water models accounting for induced polarization. The bulk aqueous solvation references for toy selectivity calculations utilizing the AMOEBA and OPLS force fields were taken to be $\Delta F^{aq}_{K\to Na} = -17.3$ kcal/mol and $\Delta F^{aq}_{K\to Na} = -18.2$ kcal/mol, respectively, as calculated in previous work (24). Above, we display the selective free energy (left panels) in naive toy models employing a (A) LJ restraint or (B) half-harmonic restraint as a function of the number of included water molecules. Our previous toy calculations (9) employing a LJ restraint and the AMOEBA water model (shown in A – blue dashed lines; open circles) are in reasonable agreement with the analogous calculations of this work (shown in A – blue solid lines; closed circles). Also shown (right panels) are the corresponding K^+/Na^+ ion-oxygen radial density functions, $\rho(r)$, and cumulative number distribution functions, $N(r)$, for the (CHARMM TIP3P) 8-water toy model (pairwise additive OPLS and polarizable AMOEBA water models gave rise to similar structural behavior). (C) Exemplary configurations for K^+ (green) and Na^+ (orange) in 8-water naive toys. Second-shell water molecules and hydrogen bond interactions are colored blue. The second-shell (2-3) water molecules around Na^+ correspond to the second peak in the Na^+-oxygen density functions [circled in A and B (right panels)].

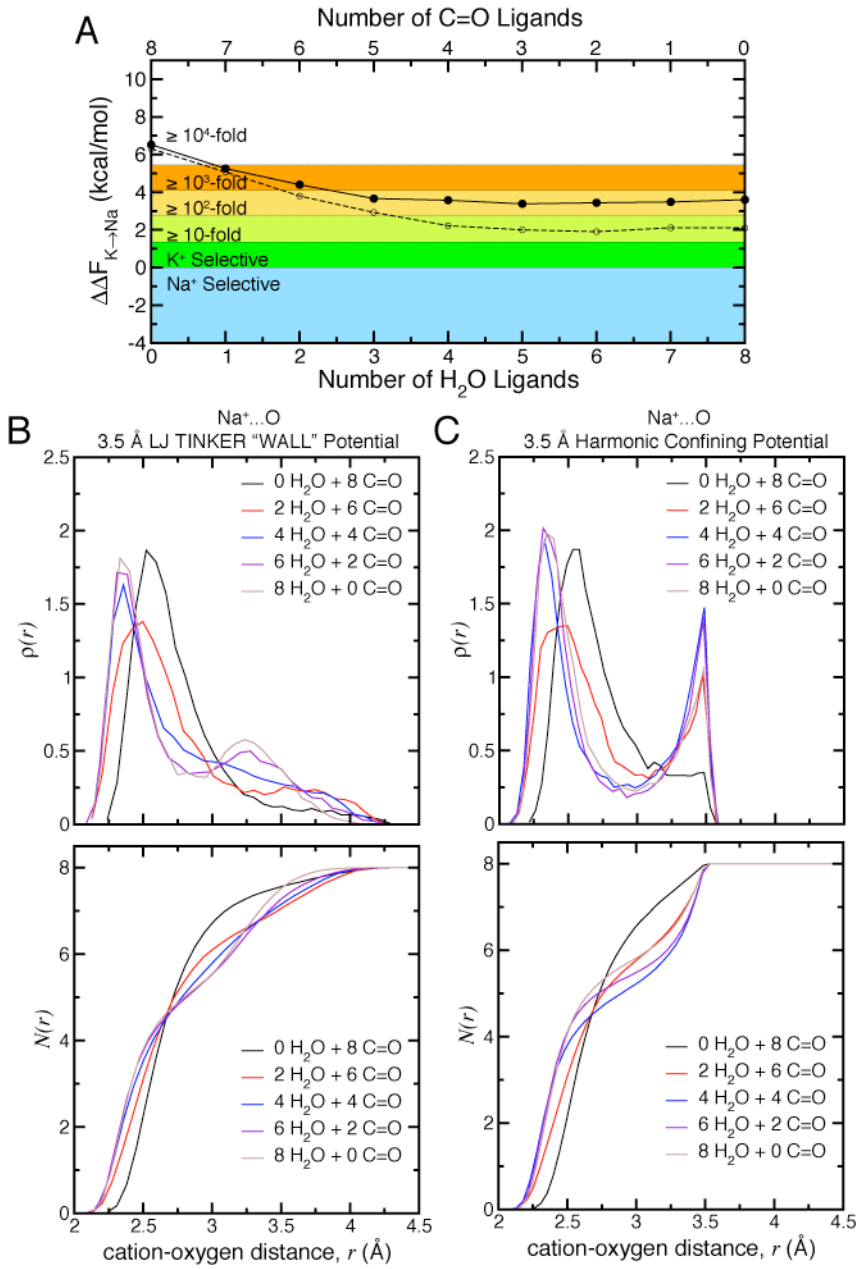

Fig S3: Selectivity and structure in naive 8-ligand toy models (3.5 Å restraint) where modified CHARMM fictitious carbonyl ligands were replaced (one-by-one) with CHARMM TIP3P water molecules (Table S2). (A) Selective free energy as a function of composition (number of included water and carbonyl moieties) in toys implementing either a LJ (solid lines/circles) or a half-harmonic (dashed lines; open circles) restraining potential. We note that although selectivity decreases as water molecules are added, positive selective free energy is seen irrespective of composition. The decrease in selectivity is not due to the larger dipole of the carbonyl groups versus water molecules, but rather to their differing molecular volume, shape, resulting charge distribution (see main text), and the resultant differences in molecular packing as enforced by U^{toy}. Fictitious linear dipolar molecules with lower assigned dipole moments (< 3 D) are, in fact, more selective than the standard carbonyl model (see main text). We also show (in B and C) Na^+-oxygen radial probability density functions (top) and cumulative number distributions (bottom) for various compositions in toys employing the (B) LJ TINKER restraint and (C) half-harmonic restraint. We note that as water molecules replace carbonyl groups, the naive toy is unable to maintain 8-fold coordination around Na^+ due to the differences in packing tendencies of the fictitious carbonyl ligands versus water molecules (see discussion in the main text).

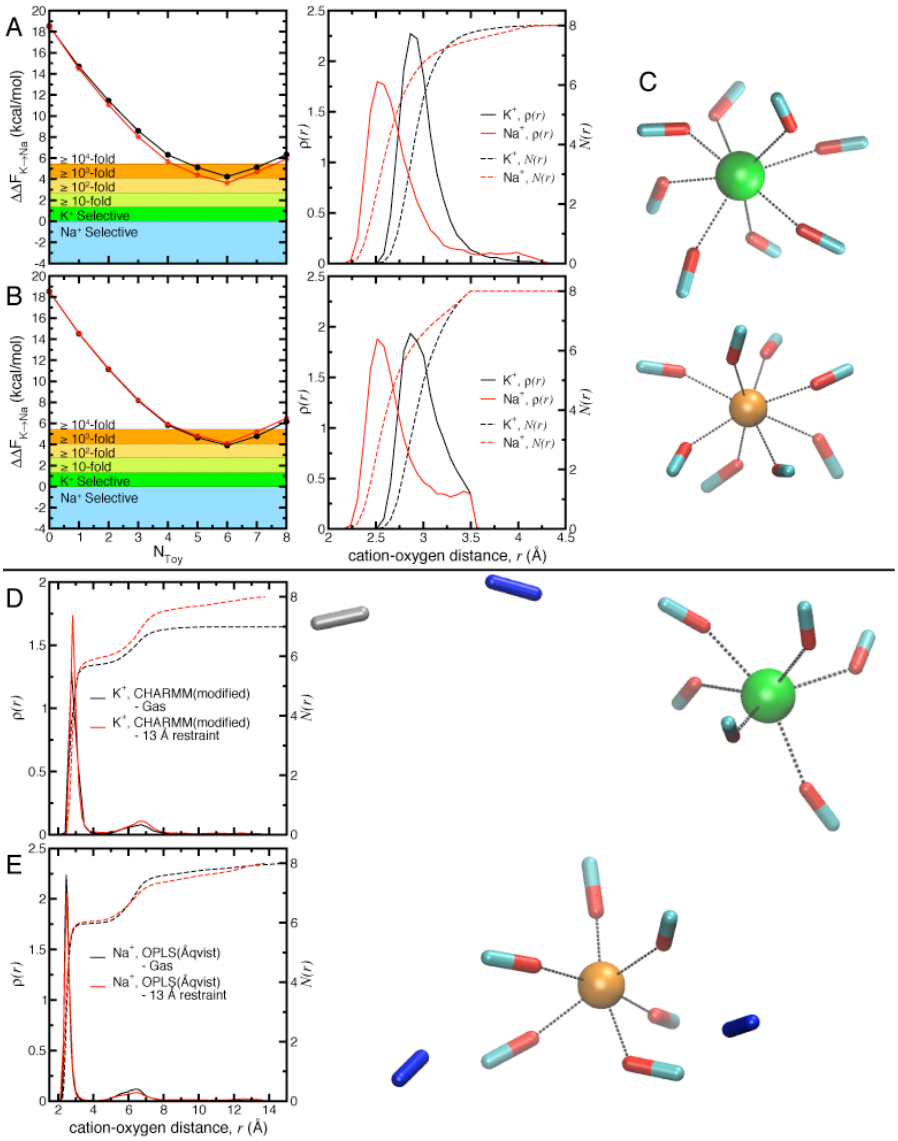

Fig S4: Fictitious carbonyl moieties in the context of different applied external fields. (A) Selectivity and structure in naive (3.5 Å) toy models and in toy models designed to enforce a single coordination shell for K^+/Na^+ (see Methods). The models employed either a (A) LJ radial restraint or (B) half-harmonic radial restraint. Selective free energy (left) is displayed as a function of N_{toy} in both the naive (3.5 Å restraint) toys (black lines; filled circles), and the toys designed to enforce N_{toy}-fold coordination (red lines; open circles). The red selective free energy data, for alchemically transforming the (LJ or half-harmonic) radial restraint (4.0→3.5 Å) and transforming $K^+ \rightarrow Na^+$ (see Methods), is not significantly different from the black selective free energy data from naive toy (3.5 Å restraint) calculations. Also shown (right panel) are the corresponding K^+/Na^+ ion-oxygen radial density functions, $\rho(r)$, and cumulative number distribution functions, $N(r)$, for the naive 8-carbonyl toy. (C) Exemplary configurations for K^+ (green) and Na^+ (orange) in 8-carbonyl naive toys. We note that, unlike water-based toys (Fig. S2) these toys successfully probe the 8-fold construct (see discussion in the main text). (D) K^+ and (E) Na^+ ion-oxygen radial density and cumulative number distribution functions for 8 carbonyls in a gas phase environment (i.e. with $U^{toy}_{K/Na} \equiv 0$) or in the presence of a radial 13 Å ion-carbonyl oxygen TINKER LJ restraint. We note that in all systems (whether the cation is K^+ or Na^+), 5-6 ligands prefer to coordinate with the central cation (as opposed to 8 in the naive toy in A and B). Also shown (right) are exemplary snapshots of K^+ (green) and Na^+ (orange) in the (13 Å LJ restraint) confined system (second shell carbonyls are blue and third shell carbonyls, silver).

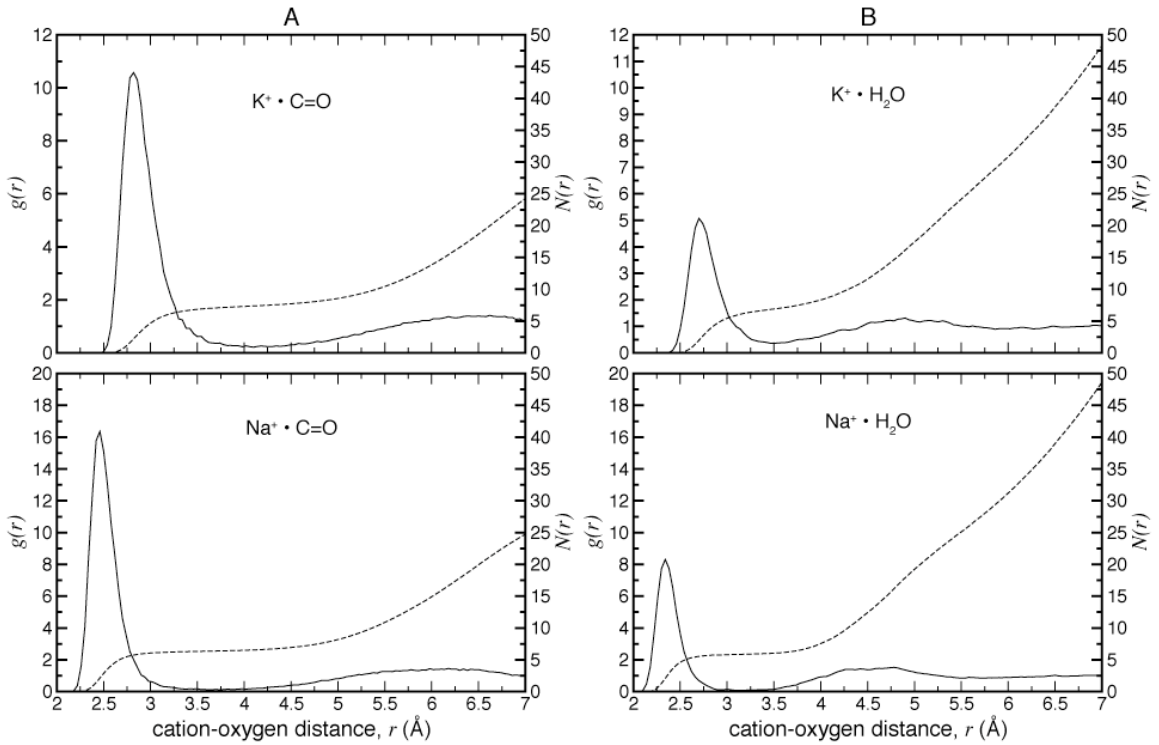

Fig S5: Structure in a bulk fluid state around ions for the carbonyl and water models investigated in this work (Table S2). Ion-oxygen pair correlation functions, $g(r)$, are shown in solid lines, and ion-oxygen cumulative number distributions, $N(r)$, are shown in dashed lines. (A) Structure of hypothetical carbonyl fluid oxygen atoms around K^+ (top panel) and Na^+ (bottom panel). The first minimum in each pair correlation function occurs at ~4.0-4.1 Å for K^+ and ~3.5-3.7 Å for Na^+. These positions correspond to a natural coordination number of ~7 for K^+ and ~6 for Na^+ in the fictitious carbonyl fluid. Note that at the largest radial position plotted, r = 7 Å, the cumulative number distributions show that ~24-25 carbonyl oxygen atoms fall within the 7 Å spherical volume around either K^+ or Na^+. (B) Structure of CHARM-TIP3P water oxygen atoms around K^+ (top panel) and Na^+ (bottom panel). The first minimum in each pair correlation function occurs at ~3.5-3.6 Å for K^+ and ~3.0-3.2 Å for Na^+. These positions correspond to a natural coordination number of ~7 for K^+ and ~6 for Na^+ in this liquid water model. At the largest radial position plotted, r = 7 Å, the cumulative number distributions show that, due to its smaller (than a hypothetical carbonyl moiety) molecular volume, ~47-48 water molecules [as opposed to ~24-25 carbonyl groups in the carbonyl fluid shown in (A)] can accommodate a 7 Å spherical volume around either K^+ or Na^+. This indicates that a carbonyl group naturally occupies approximately 2 times as much volume as a water molecule.

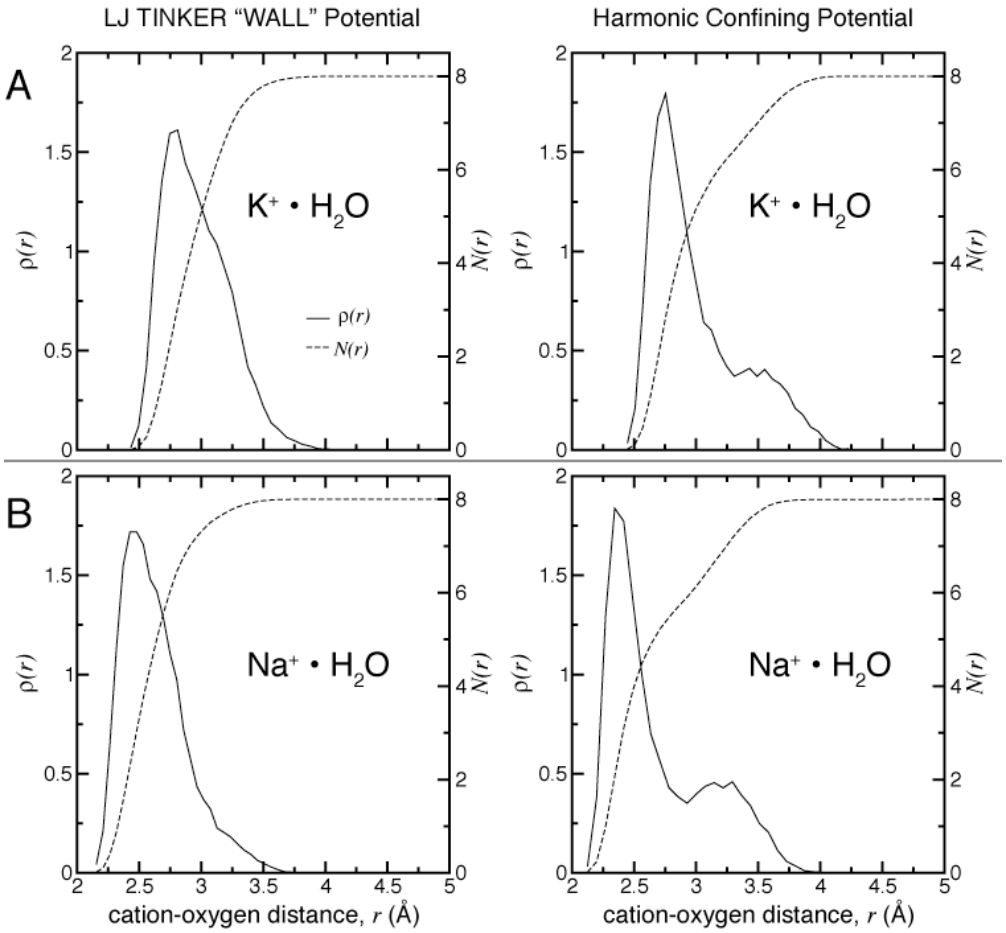

Fig S6: Ion-oxygen radial probability density, $\rho(r)$ (solid lines), and cumulative number distribution, $N(r)$ (dashed lines) for (A) K^+ and (B) Na^+ in 8-water toy models where where $U^{toy}_{K/Na}$ is a volume constraint designed to suppress formation of secondary solvation shells around the central cation (see Methods). Left and right panels display results obtained with LJ and (5 kcal/mol/Å^2) half-harmonic volume confining restraints, respectively. The radial restraint was set at 3.0 Å and 3.5 Å in the cases of Na^+ and K^+, respectively. We note that the toys implementing a LJ TINKER restraint (left) appear to better suppress formation of a second solvation shell than those implementing a half-harmonic restraint (right). Nonetheless, all models in this class largely enhanced the propensity for observing 8 nearest neighbors for the central cation in comparison to the naive model (Figs. S2-S3). The K^+ selective free energy for these toy models as a function of N_{toy} is displayed in Fig. 4D.

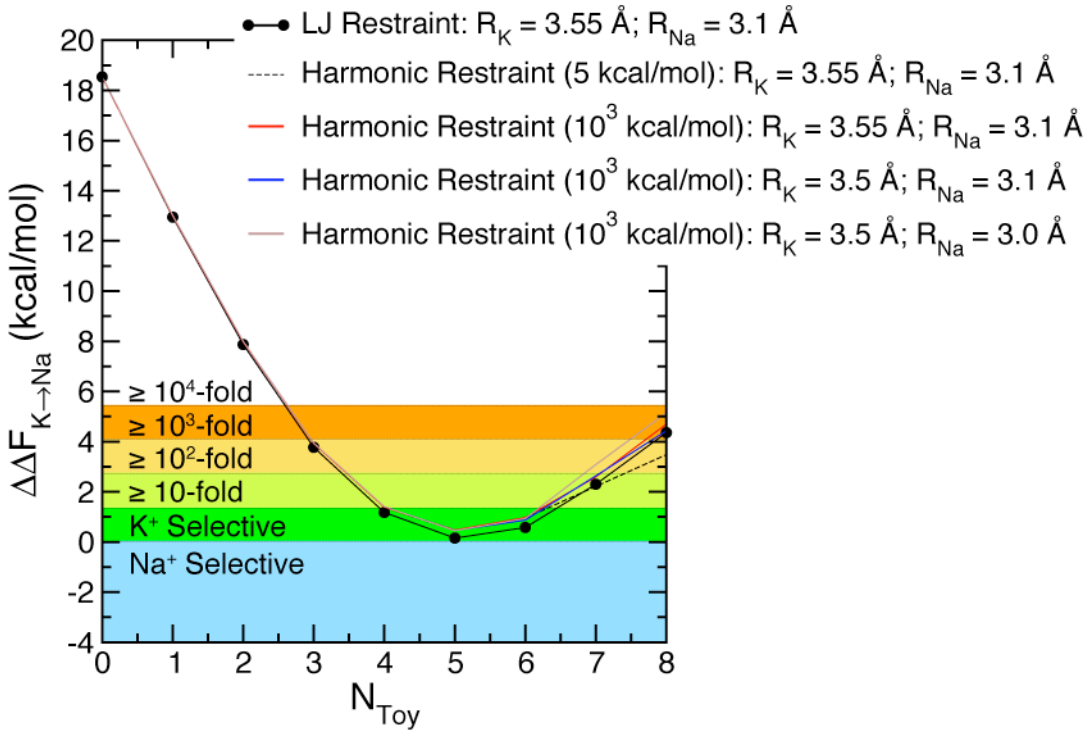

Fig S7: Examples of various water-based trial toy models where the ion-water radial restraint (R_K and R_{Na} for K^+ and Na^+, respectively) was alchemically transformed depending on the central ion type (see Methods). All toys implemented either a TINKER LJ or half-harmonic restraint. Though all radius pairs (R_K, R_{Na}), were chosen based on the cation-oxygen pair correlation analyses in Fig. S5, we note that the LJ-based models [just as seen in Fig. S6 (left)] were better able to suppress formation of secondary solvation shells for both K^+ and Na^+.

References

1. MacKerrel Jr., A. D. 1998. All-atom Empirical Potential for Molecular Modeling and Dynamics Studies of Proteins. J. Phys. Chem. B. 102:3586-3616.
2. Bernèche, S. and B. Roux. 2001. Energetics of Ion Conduction through the K^+ Channel. Nature 414:73-77.
3. Roux, B. and S. Bernèche. 2002. On the Potential Functions Used in Molecular Dynamics Simulations of Ion Channels. Biophys. J. 82:1677-1684.
4. Jorgensen, W. L., J. Chandrasekhar, and J. D. Madura. 1983. Comparison of Simple Potential Functions for Simulating Liquid Water. J. Chem. Phys. 79:926-935.
5. Noskov, S. Y., S. Bernèche, and B. Roux. 2004. Control of ion Selectivity in Potassium Channels by Electrostatic and Dynamic Properties of Carbonyl Ligands. Nature 431:830-834.
6. Noskov, S. Y. and B. Roux. 2007. Importance of Hydration and Dynamics on the Selectivity of the KcsA and NaK Channels. J. Gen. Physiol. 129:135-143.
7. Noskov, S. Y. and B. Roux. 2006. Ion Selectivity in Potassium Channels. Biophys. Chem. 124:279-291.
8. Ponder, J. W. 2004. TINKER: Software Tools for Molecular Design. Version 4.2. Saint Louis, MO.
9. Bostick, D. L. and C. L. Brooks III. 2007. Selectivity in K^+ Channels is Due to Topological Control of the Permeant Ion's Coordinated State. Proc. Natl. Acad. Sci. U. S. A. 104:9260-9265.
10. Asthagiri, D. and L. R. Pratt. 2006. Role of Fluctuations in a Snug-Fit Mechanism of KcsA Channel Selectivity. The Journal of Chemical Physics 125:024701.
11. Fowler, P. W., K. Tai, and M. S. P. Sansom. 2008. The Selectivity of K^+ Ion Channels: Testing the Hypotheses. Biophys. J. 95:5062-5072.
12. Bostick, D. L. and C. L. Brooks III. 2008. The Statistical Determinants of Selective Ionic Complexation: Ions in Solvent, Transport Proteins, and Other 'Hosts'. Biophys. J. submitted.
13. Berendsen, H. J. C., D. van der Spoel, and R. van Drunen. 1995. GROMACS: A Message-passing Parallel Molecular Dynamics Implementation. Comput. Phys. Commun. 91:43-56.
14. Lindahl, E., B. Hess, and D. van der Spoel. 2001. Gromacs 3.0: A Package for Molecular Simulation and Trajectory Analysis. Journal of Molecular Modeling 7:306-317.
15. Essmann, U., L. Perera, M. L. Berkowitz, T. Darden, H. Lee, and L. Pedersen. 1995. A Smooth Particle Mesh Ewald Method. J. Chem. Phys. 103:8577-8593.
16. Nose, S. and M. L. Klein. 1983. Constant Pressure Molecular Dynamics for Molecular Systems. Mol. Phys. 50:1055-1076.
17. Parrinello, M. and A. Rahman. 1981. Polymorphic Transitions in Single Crystals: A New Molecular Dynamics Method. J. Appl. Phys. 52:7182-7190.
18. Latorre, R. and C. Miller. 1983. Conduction and Selectivity in Potassium Channels. J. Membr. Biol. 71:11-30.

19. Lockless, S. W., M. Zhou, and R. MacKinnon. 2007. Structural and Thermodynamic Properties of Selective Ion Binding in a K^+ Channel. PLoS Biology 5:e121/1079-1088.
20. Yellen, G. 1984. Ionic Permeation and Blockade in Ca^{2+}-activated K^+ Channels of Bovine Chromaffin Cells. J. Gen. Physiol. 84:157-186.
21. Neyton, J. and C. Miller. 1988. Potassium Blocks Barium Permeation through a Calcium-activated Potassium Channel. J. Gen. Physiol. 92:549-567.
22. LeMasurier, M., L. Heginbotham, and C. Miller. 2001. KcsA: It's a Potassium Channel. J. Gen. Physiol. 118:303-313.
23. Åqvist, J. 1990. Ion-Water Interaction Potentials Derived from Free Energy Perturbation Simulations. J. Phys. Chem. 94:8021-8024.
24. Grossfield, A., P. Ren, and J. W. Ponder. 2003. Ion Solvation Thermodynamics from Simulation with a Polarizable Force Field. J. Am. Chem. Soc. 125:15671-15682.
25. Ren, P. and J. W. Ponder. 2003. Polarizable Atomic Multipole Water Model for Molecular Mechanics Simulation. J. Phys. Chem. B. 107:5933-5947.